

Importance of reference Hamiltonians containing exact exchange for accurate one-shot GW calculations of Cu_2O

Leah Y. Isseroff¹ and Emily A. Carter^{2,*}¹*Department of Chemical and Biological Engineering, Princeton University, Princeton, New Jersey 08544-5263, USA*²*Department of Mechanical and Aerospace Engineering, Program in Applied and Computational Mathematics, and Andlinger Center for Energy and the Environment, Princeton University, Princeton, New Jersey 08544-5263, USA*

(Received 17 January 2012; revised manuscript received 10 April 2012; published 22 June 2012)

We show that a “one-shot” GW approach (denoted G_0W_0) can accurately calculate the photoemission/inverse-photoemission properties of Cu_2O . As the results of any perturbative method are heavily dependent on the reference state, the appropriate reference Hamiltonian for G_0W_0 is identified by evaluating the performance of density-functional-theory-based input wave functions and eigenvalues generated with selected exchange-correlation functionals. It is shown that a reference Hamiltonian employing the hybrid Heyd-Scuseria-Ernzerhof functional used in conjunction with G_0W_0 produces an accurate photoemission/inverse-photoemission band gap and photoemission spectrum whose character is then further analyzed. The physical origin of why a hybrid functional is required for the zeroth-order wave function is discussed, giving insight into the unique electronic structure of Cu_2O in comparison to other transition-metal oxides.

DOI: [10.1103/PhysRevB.85.235142](https://doi.org/10.1103/PhysRevB.85.235142)

PACS number(s): 71.15.Qe, 82.45.Vp, 79.60.-i, 77.22.Ch

I. INTRODUCTION

Cu_2O is a p -type semiconductor that is attractive for use in photovoltaics and photocatalysis due to its abundance, nontoxicity, and low-cost production processing. Its band gap of 2.17 eV falls within a spectral range near the solar maximum,¹ rendering it an excellent absorber of sunlight, and the estimated position of its conduction band provides a large overpotential for reduction reactions involved in water splitting and carbon dioxide reduction.² Its catalytic potential is also evident from the widespread use of copper-based and copper-oxide-based catalysts in commercial chemical reactions, including the Cu/ZnO catalyst used for methanol production from CO and H_2 ,³ and the CuO/ZrO_2 catalyst used for low-temperature CO oxidation.⁴ Experimentally, Cu_2O has been effective in photocatalytic water splitting, albeit with low efficiencies,^{5,6} and it shows promise to be functional in CO_2 reduction.^{7,8} Cu_2O has also been used as the p -type material in heterojunction solar cells, but with efficiencies of less than 2%. Its poor performance highlights the need to optimize its properties for solar energy conversion through alloying or doping with other elements.

Directed materials design can be facilitated through quantum-mechanical studies, using well-founded theoretical approaches to calculate the relevant properties of Cu_2O -based materials and to evaluate how they may perform in photocatalysis. Two important measures of functionality are efficient absorption of sunlight and band-edge energies placed favorably for electrochemistry. A fundamental step in the verification of both of these properties is the assessment of the photoemission/inverse-photoemission spectrum (PES/IPES).⁹

Accurate theoretical calculations of the PES/IPES are also significant as the first step in a multistep process to calculate the optical absorption spectrum (OAS). The OAS of Cu_2O has been of considerable interest for decades as the prototype of Wannier excitons,¹⁰ and while the spectrum has been well-studied experimentally,^{1,11} theoretical approaches are required for full characterization of all optical transitions. Finding an

accurate means of calculating the PES/IPES is thus crucial not only for photocatalytic design applications, but it also opens the door for detailed study of the OAS.

The PES/IPES can be derived from many-body perturbative Green’s function methods, which are used to calculate electronic quasiparticle excitations. In the Hamiltonians of these methods, the exchange-correlation self-energy accounts for all nonclassical electronic interactions, but its exact expression as formulated in Hedin’s equations is intractable even for simple systems.¹² The standard means for evaluating the self-energy is the GW approximation,¹² where the common practice is to use a “one-shot” method (denoted G_0W_0) that is a first-order correction to a reference single-particle Hamiltonian, H_0 . Other schemes for GW calculations with varying levels of self-consistency have also been developed.^{13–17}

One of the most successful self-consistent approaches is the quasiparticle self-consistent GW (QS GW) approximation, in which a static, Hermitian, one-body Hamiltonian is constructed to minimize a measure of difference between its effective potential and the self-energy.^{16,17} In each iteration of QS GW , a GW calculation is performed and the resulting self-energy is recast as a Hermitian Hamiltonian that is used for the next iteration. Essentially, this formulation constructs a reference Hamiltonian that reduces the perturbation in a final one-shot G_0W_0 calculation. Although QS GW has been successful in improving the band structure for many materials where standard G_0W_0 methods have failed, it has a tendency to overestimate band gaps. This may result from neglecting the vertex function when applying self-consistency, which, if retained, would incorporate higher-order electron-electron interactions in every iteration. A true self-consistent solution of Hedin’s equations would include the vertex function in every iteration—in the expression for the self-energy, where within the GW approximation the vertex function is fixed (to δ functions), and in the screened Coulomb interaction W , which is approximated within the random phase approximation (RPA).¹⁸ By neglecting the vertex function, the implementation of self-consistent GW becomes conceptually

inconsistent with the true self-consistent solution to Hedin's equations. Unless vertex corrections are incorporated within each iteration (which have been difficult to account for in the construction of both W and the self-energy¹⁹), it is inconclusive whether self-consistency is more reliable than a zeroth-order GW calculation from a good Kohn-Sham reference. Additionally, there is no mathematical proof that the QSGW approach is truly independent of the initial Hamiltonian, and the question remains if its solution is truly unique.

Bruneval *et al.* applied the GW approximation with varying levels of self-consistency to calculate quasiparticle excitations of Cu_2O .²⁰ They reported that the standard G_0W_0 approach failed and predicted a gap far below the experimental value, and they showed that the QSGW approach calculated a more accurate gap. However, due to the reasons described previously, it may be more conceptually sound to improve the choice of reference Hamiltonian through Kohn-Sham methods and then use the standard one-shot G_0W_0 approach, as opposed to improving the reference Hamiltonian through the constrained approximation to self-consistency in QSGW. Additionally, the dependence on QSGW is problematic due to the prohibitive expense introduced by self-consistency, which can be a hindrance for further computational evaluation of Cu_2O -based photocatalytic materials. For these reasons, we aim to develop an alternative approach within the framework of the standard G_0W_0 calculation, seeking to establish an accurate method that is both well-justified and computationally tractable.

The success of the G_0W_0 method depends heavily on the accuracy of the reference single-particle Hamiltonian, H_0 . In the one-shot approach, G_0 and W_0 are calculated from the reference eigenvalues and eigenfunctions, and a single GW iteration cannot be expected to correct an eigenvalue gap that is not of the same order of the experimental gap. The inaccurate G_0W_0 calculation reported by Bruneval *et al.* used Kohn-Sham density functional theory (DFT) as the reference Hamiltonian, with an exchange-correlation (XC) functional employing the local density approximation (LDA).²⁰ The failure of G_0W_0 there was likely due to the inaccuracy of the LDA functional, because local treatment of electron XC does not capture the physics of strongly correlated electrons, inadequately describing the strong electron repulsion of the localized d electrons in first-row, mid-to-late transition-metal oxides.²¹ The failure of the LDA+ G_0W_0 approach is an indication that the large errors of the reference Hamiltonian could not be corrected perturbatively. To enable an accurate G_0W_0 method, it is therefore necessary to first determine an H_0 with an XC functional that will appropriately treat the ground-state properties of the material under study. Bruneval *et al.* chose to construct a more accurate H_0 through the QSGW method, which showed significant improvements over the LDA+ G_0W_0 results. However, due to the previously explained rationale, we choose to employ DFT-based methods for the H_0 . This strategy has been used successfully in modeling the PES/IPES of hematite.²²

One approach to correcting the failure of local and semilocal XC functionals is the DFT+ U method,^{23,24} which introduces a parametrized Hartree-Fock (HF)-like potential to describe on-site interactions of highly localized electrons, such as d or f

electrons. In many systems, DFT+ U produces a better mean-field description than DFT with either the generalized gradient approximation (GGA) or LDA XC functionals, and combined DFT+ U + G_0W_0 approaches have shown improvement in the predicted band structures in comparison with standard DFT+ G_0W_0 methods.^{22,25,26}

For systems in which the on-site approximate treatment of exact exchange in DFT+ U does not accurately describe all electron-electron interactions, it may be necessary to incorporate exact exchange from the HF formalism into the XC functional applied to all electrons, through the use of hybrid functionals. The Perdew-Burke-Ernzerhof hybrid (PBE0)²⁷ and the Heyd-Scuseria-Ernzerhof (HSE) functionals²⁸⁻³¹ are examples of hybrid functionals that accurately predict a number of ground-state properties of strongly correlated systems, and thus may be appropriate for use in the reference Hamiltonian of a G_0W_0 calculation. Both replace a portion of PBE GGA^{32,33} exchange with HF exchange, leaving correlation to be fully treated by the PBE GGA functional. HSE contains a nonlocal screened-exchange portion of its functional that functions similarly to the nonlocal and screened self-energy operator in the GW approximation. Therefore, the HSE functional itself is a reasonable zeroth-order approximation of the self-energy, and its use is a step toward a level of self-consistency without employing a fully self-consistent GW method. A combined HSE+ G_0W_0 approach has been used to accurately calculate quasiparticle gaps and spectra for a number of transition-metal oxides,³⁴ but not for Cu_2O .

The paper is organized as follows. In Sec. II, we describe the computational details of all first-principles methods employed here. Section III presents and discusses numerical results, beginning by analyzing the accuracy of DFT, DFT+ U , and DFT with hybrid functionals to treat Cu_2O . In addition to determining an accurate H_0 for G_0W_0 , this also establishes a foundation for related ground-state studies of Cu_2O (i.e., surface chemistry related to reaction catalysis). The section concludes with an evaluation of a number of functionals as reference Hamiltonians in subsequent G_0W_0 calculations, with the resulting quasiparticle spectra analyzed in detail. Finally, conclusions are summarized in Sec. IV.

II. COMPUTATIONAL DETAILS

DFT, DFT+ U , and GW calculations were done using the Vienna Ab-initio Simulation Package (VASP version 5.2.2),³⁵ using Blöchl's all-electron, frozen-core projector augmented wave (PAW) method to represent the nuclei and core electrons, and leaving 11 valence electrons of Cu (or 17 electrons when studying the effect of including the semicore Cu $3p$ electrons) and six valence electrons of O to be treated self-consistently. All PAW potentials were obtained from the VASP package; the standard PAW potential was used for O. A cubic unit cell containing six atoms (two formula units of Cu_2O) was used, and the cell's equilibrium volume and bulk modulus were found with each of the DFT-based theories by fitting a computed energy-volume curve to the Murnaghan equation of state.³⁶ The cell shape and atom positions were fixed to the cuprite structure (space group $Pn3m$, No. 224). A Γ -point-centered k -point mesh of $6\times 6\times 6$ was used (corresponding to 20 irreducible k points), with a plane-wave kinetic energy cutoff of 700 eV, both of which converged the total energy to

within 1 meV/atom. Brillouin zone integration employed the tetrahedron method with Blöchl corrections.³⁷ The exchange-correlation functionals used in both DFT and DFT+ U calculations were the LDA with the Ceperley-Alder³⁸ exchange-correlation as parametrized by Perdew and Zunger,³⁹ and PBE GGA. The formalism of Dudarev *et al.*⁴⁰ was used for DFT+ U , testing a range of U - J values from 2 to 8 eV for both LDA+ U and PBE+ U to determine the optimal value that delivered the most accurate ground-state properties. The hybrid functionals used here were PBE0 and HSE, where HSE was used with a screening parameter of 0.2 Å⁻¹ in conformance with the value recommended by Krukau *et al.*⁴¹ The HF kernel for hybrid functionals is evaluated on a subgrid of k points that is denoted the q -point mesh, which was down-sampled from the full Γ -point-centered $6\times 6\times 6$ grid to $2\times 2\times 2$ to decrease the high computational cost of the full HF kernel calculation. Evaluation of errors due to downsampling is discussed in the next section.

The calculation of the dielectric response function for GW used a reduced Γ -point-centered q -point mesh of $3\times 3\times 3$. The converged number of bands was 64 when subsuming the semicore electrons into the frozen core of the PAW potential, whereas 112 bands were used when treating the semicore electrons self-consistently. A total of 64 frequency points were used to evaluate the dielectric response function. These parameters resulted in quasiparticle gaps that were converged to within 0.1 eV.

III. RESULTS AND DISCUSSION

A. DFT, DFT+ U , and hybrid functional calculations of ground-state properties

To evaluate the accuracy of each functional, a set of observables was calculated by quantum calculations, and the obtained values were compared to experiment. The first two

observables are the equilibrium lattice constant and the bulk modulus. Two additional observables considered were the photoemission spectrum peaks and the PE/IPE band gap, both of which characterize electronic properties of the system. Photoemission spectra of Cu₂O exhibit six different peaks—the oxygen-related features A and B , and the Cu-related features C - F .⁴² These peak energies are used for comparison to peaks in densities of states (DOSs) calculated with each functional at the material's corresponding equilibrium geometry. While it is possible to compare the DOS conduction band peaks to the three IPES peaks identified by Ghijssen *et al.*,⁴³ calculated DOS conduction band peak energies will be significantly shifted as a result of any error in the band-gap energy (whose value is extremely sensitive to the XC functional used), so this comparison is not a strong metric for evaluation of accuracy. Instead, we use the IPE DOS only to determine the IPE onset (i.e., the conduction band edge), which then defines the PE/IPE gap. Although the PE/IPE band gap cannot be predicted precisely using the eigenvalue gap obtained from a ground-state DFT calculation, it can still be expected to be of the same order, and must be so for the first-order G_0W_0 correction to be effective. This eigenvalue gap comparison is made here as another evaluation of the accuracy of the electronic structure. These four calculated observables for the LDA, LDA+ U , PBE, PBE+ U , PBE0, and HSE functionals are compared with experimental values in Table I.

The accuracy of each functional can be evaluated from the results presented in Table I. The LDA DOS peaks here differ slightly from those in Ref. 20, most likely due to their use of the experimental lattice parameter for the geometries, whereas in this study the structure was determined from first principles so that the entire calculation is internally consistent and independent of experimental input. Additional sources of variation are their explicit treatment of the Cu $3s\ 3p$

TABLE I. Calculated equilibrium lattice constant, bulk modulus, DOS peaks, and eigenvalue gap using DFT, DFT+ U , and DFT with hybrid XC functionals. For DFT+ U , both the LDA and PBE functionals were used, with a range of U - J values. Results are compared to measured values.

Functional	U - J value (eV)	Equilibrium lattice constant (Å)	Bulk modulus (GPa)	DOS peaks						Eigenvalue gap (eV)
				A	B	C	D	E	F	
LDA	N/A	4.1814	145	-7.75	-6.0	-2.5	-1.95	-1.4	-0.6	0.68
LDA+ U	2	4.1657	143	-7.7	-5.9	-2.8	-2.25	-1.5	-0.6	0.81
	4	4.1475	141	-7.55	-5.75	-3.1	-2.5	-1.6	-0.7	0.92
	6	4.1258	137	-7.6	-5.7	-3.5	-2.8	-1.7	-0.7	1.04
	8	4.1000	135	-7.75	-5.75	-3.8	-3.2	-1.75	-0.75	1.15
PBE	N/A	4.3123	109	-6.5	-5.0	-2.0	-1.5	-1.1	-0.5	0.43
PBE+ U	2	4.3013	106	-6.8	-5.2	-2.45	-1.8	-1.3	-0.6	0.54
	4	4.2887	103	-6.75	-5.0	-2.75	-2.4	-1.45	-0.6	0.65
	6	4.2738	100	-6.6	-4.9	-3.0	-2.5	-1.5	-0.6	0.74
	8	4.2557	96	-6.7	-5.0	-3.4	-2.8	-1.5	-0.6	0.84
PBE0	N/A	4.2851	114	-7.4	-5.75	-2.9	-2.5	-1.7	-0.5	2.84
HSE	N/A	4.2887	114	-7.45	-5.8	-3.0	-2.45	-1.9	-0.7	2.04
Experimental	N/A	4.2696 ^a	112 ^b	-7.3 ^c	-6.0 ^c	-3.5 ^c	-3.0 ^c	-2.0 ^c	-1.0 ^c	2.17 ^d

^aReference 49.

^bReference 50.

^cReference 42.

^dPE/IPE gap from Ref. 1.

semicore electrons, whereas here the Cu semicore electrons were subsumed in the PAW potential, as well as their shifting of removal energies using peak D as a reference, whereas here electron removal energies were all referenced to the valence band maximum in each calculation. It is evident that the LDA and LDA+ U fail in calculating the structural properties, both underestimating the lattice constant by 2–4% and overestimating the bulk modulus by 20–30%, and also calculating eigenvalue gaps that are 45–78% lower than the observed PE/IPE gap. These failures indicate that the LDA family of XC functionals is inappropriate for any ground-state DFT calculations of Cu_2O material properties, as well as for the reference Hamiltonian for G_0W_0 .

Our results using the PBE functional agree well with previously published predictions,⁴⁴ and show some improvement over the LDA results. PBE calculates a lattice constant just 1% larger than the experimental value and reproduces well the measured bulk modulus, although it more severely underestimates (by 80%) the eigenvalue gap than the LDA functional does. The PBE+ U functional improves upon these results, opening up the gap further to a maximum of nearly 40% of the true value, with greater accuracy in predicting the equilibrium geometry, but at the cost of a 10%-less-accurate bulk modulus. Additionally, the PBE functionals inaccurately produce a shift in the oxygen-related features A and B of nearly 1 eV, relative to both LDA and experimental values. Although none of the PBE+ U results are wholly satisfying, one can identify an optimal value for $U-J$ in PBE+ U at 6 eV, based solely on its accuracy in predicting the equilibrium lattice constant. (This value differs from previous DFT+ U studies of Cu_2O , where a value of 7 eV was chosen based on a fit to experimental data of CuO).⁴⁵

The failure of the DFT+ U method to open up the gap sufficiently can be understood by studying the character of the valence and conduction bands, shown in the projected DOS in Fig. 1. The character of the valence band in Cu_2O is not purely Cu $3d$, but also contains contributions from the O $2p$ and Cu $4s$ states, and the conduction band also has mixed Cu $3d$, Cu

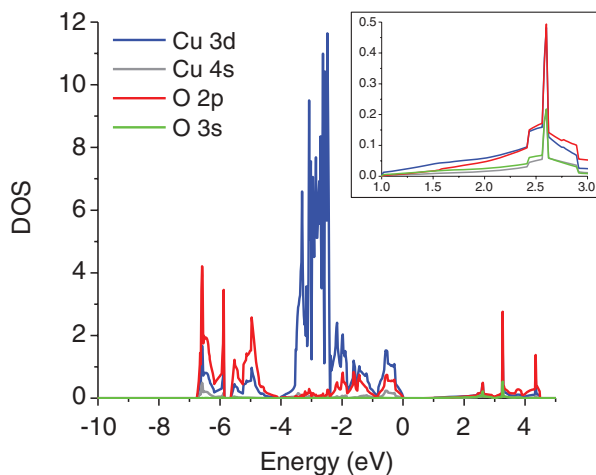


FIG. 1. (Color online) Projected density of states obtained from a PBE+ U calculation, where the value of $U-J$ is 6 eV. The inset shows a more refined view of the character at the edge of the conduction band.

$4s$, and O $3s$ character. DFT+ U only applies the parametrized potential to intra-atomic interactions of electrons of a specified angular momentum, which were chosen here to be the Cu $3d$ electrons, and it treats the interactions between these electrons and the rest of the system via the standard DFT formalism. This limited correction implies that other orbitals' contributions to the band edges will inhibit the ability of the added approximate exchange to significantly shift the band-edge energies and open up the gap. The failure of DFT+ U here highlights the need to apply a form of exact exchange not only to the selected localized electrons, but also to the interactions of all electrons in the system.

HF exchange was incorporated in DFT calculations by using the hybrid functionals PBE0 and HSE. Down-sampling of the HF q -point mesh resulted in an eigenvalue gap difference of 0.17 eV for PBE0 and 0.09 eV for HSE, with a variability in the lattice constant of $<0.2\%$, relative to test calculations conducted without down-sampling. The smaller impact of down-sampling with the HSE functional is due to the screening in the HSE functional, which allows for faster convergence with respect to k -point mesh size.⁴⁶ While this shows that the HSE functional is more stable when down-sampling, the effect of down-sampling on PBE0 results was still small enough to justify its use to achieve lower computational expense. Hybrid DFT results using a $2 \times 2 \times 2$ q -point mesh for both HSE and PBE0 functionals are also shown in Table I.

Both PBE0 and HSE perform equally well in calculating the equilibrium lattice constant and the bulk modulus, and their DOS peak positions are also very similar. However, the HSE functional performs better in producing an eigenvalue gap that is closer to the PE/IPE gap, indicating an advantage of using HSE over PBE0. For this reason, in addition to its greater stability when down-sampling the q -point mesh, the HSE functional with a q -point mesh of $2 \times 2 \times 2$ can be selected as the optimal approach for ground-state calculations of Cu_2O .

B. G_0W_0 calculations of the quasiparticle spectrum

The accuracy of the HSE functional signifies its potential as a reference Hamiltonian in G_0W_0 calculations, but to compare the effect of various reference Hamiltonians on the resulting G_0W_0 observables, G_0W_0 was done with wave function and eigenvalue input from four of the most promising ground-state XC functionals, specifically PBE, PBE+ U , PBE0, and HSE. Additionally, because it was maintained in the earlier study that the explicit inclusion of the semicore states in the GW calculation was needed to predict the semiconductor character of the material,²⁰ the effect of inclusion of the Cu $3p$ electrons was also evaluated. The results from each combined $H_0+G_0W_0$ approach are displayed in Table II, where here only the quasiparticle peaks and gaps are compared to the experimental values (the GW approach as implemented in VASP cannot give total energies, making it incapable of calculating observables such as geometries or bulk moduli).

It is evident from Table II that the most accurate H_0 leads to the most accurate G_0W_0 predictions. Because the HSE-derived observables were already extremely accurate, the first-order correction of G_0W_0 does not deviate strongly, resulting in a quasiparticle gap that is closest to the experimental gap and in electron energy removal energies that compare fairly

TABLE II. Quasiparticle peaks and gaps (eV) as calculated with the G_0W_0 method, comparing the effects of selected DFT methods used as the reference Hamiltonian. Values in parentheses were calculated treating Cu semicore electrons explicitly.

Functional	Quasiparticle peaks (electron removal energies)						Quasiparticle gap (eV)
	A	B	C	D	E	F	
PBE	-6.75 (-7.2)	-5.5 (-5.8)	-2.3 (-2.5)	-1.8 (-1.8)	-1.3 (-1.25)	-0.55 (-0.6)	1.39 (1.54)
PBE+ U	-7.0 (-7.5)	-5.55 (-6.0)	-2.8 (-2.8)	-2.3 (-2.1)	-1.5 (-1.6)	-0.6 (-0.6)	1.85 (1.76)
PBE0	-7.45 (-7.6)	-6.0 (-6.1)	-2.9 (-2.9)	-2.4 (-2.2)	-1.6 (-1.7)	-0.6 (-0.6)	2.52 (2.36)
HSE	-7.3 (-7.5)	-5.9 (-6.1)	-2.75 (-2.8)	-2.1 (-2.2)	-1.5 (-1.5)	-0.5 (-0.6)	2.17 (2.02)
Experimental values	-7.3 ^a	-6.0 ^a	-3.5 ^a	-3.0 ^a	-2.0 ^a	-1.0 ^a	2.17 ^b

^aReference 42.

^bPE/IPE gap from Ref. 1.

well to experimental values. For other H_0 functionals, the G_0W_0 perturbation does shift all observables somewhat closer to the experimental values, but improvement in accuracy is limited. For example, PBE0+ G_0W_0 continues to overestimate the quasiparticle gap, and PBE+ G_0W_0 and PBE+ U + G_0W_0 both continue to underestimate it. These results differ from the conclusions obtained from the study of GW approaches for hematite,²² where DFT+ U + G_0W_0 was determined to be the method of choice, highlighting the importance of identifying a material-specific optimal H_0 . In particular, the nature of the band edges determines whether DFT+ U suffices: DFT+ U + G_0W_0 underestimates the quasiparticle gap for Cu_2O due to the mixed character at the band edges that requires all electrons be treated with exact exchange, not just the d electrons as in the DFT+ U treatment. By contrast, the conduction band in hematite is strongly dominated by Fe $3d$ character, and so DFT+ U + G_0W_0 is effective.

This hybridization within the valence band highlights cuprous oxide's unique character due to its unusual structure. Cu_2O consists of a cubic phase formed by two interpenetrating crystalalite-like networks, differing from the many more-closely-packed transition-metal oxides. The stability of the cubic phase over a competing less dense crystalalite-like structure is dependent on attractive Cu-Cu interactions between the two sublattices.⁴⁷ These interactions have been

suggested to be of a covalent nature (stemming from a charge transfer from Cu $3d$ orbitals to $4s$ and $4p$ orbitals higher in energy)⁴⁷ or weakly metallic cation-cation bonding (from partially occupied Cu $4s$ and $4p$ orbitals as a result of the partial ionization of the Cu and O ions).⁴⁸ It is this mixed character in the valence and conduction bands that necessitates the use of hybrid functionals, which apply exact exchange to all electrons in the system, most significantly to those electrons that are not Cu $3d$ that also contribute to the character of the band edges. The suitability of HSE+ G_0W_0 may be extended to similar transition-metal oxides where hybridization occurs in the band edges.

It was reported previously that subsuming the semicore electrons into the PAW potential led to a metallic description for Cu_2O using GW with an LDA H_0 ,²⁰ but we do not see this behavior here. Inclusion of the Cu semicore states is observed to most strongly affect the electron removal energies of the O $2p$ electrons for PBE and PBE+ U (peaks A and B), but the effect on the hybrid functional quasiparticle energies and on all quasiparticle gaps shows differences smaller than 0.2 eV. Thus in the less accurate levels of theory, the semicore electrons have a strong impact on the accuracy of the results; however, when the functional used is already sufficiently accurate, the impact is minimal, and the computational expense of their explicit treatment can be avoided.

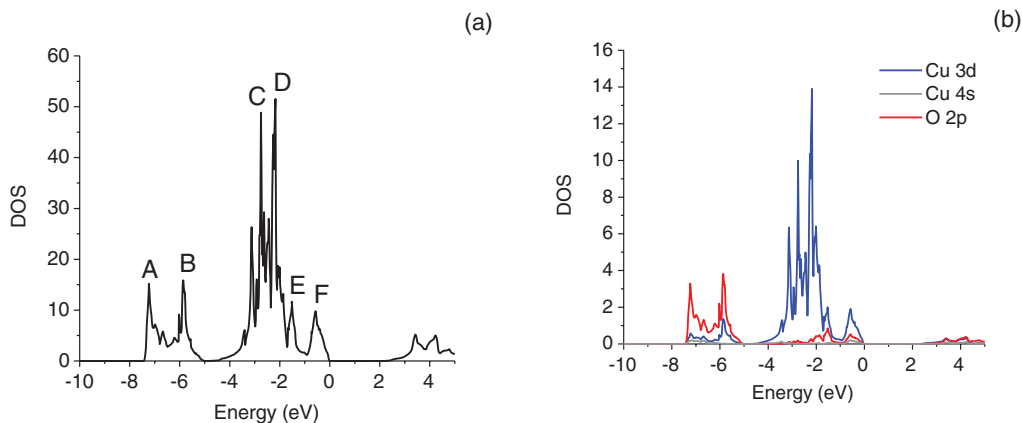


FIG. 2. (Color online) Quasiparticle spectrum obtained from the HSE+ G_0W_0 calculation. Panel (a) shows the total density of states, with the features corresponding to experimentally observed photoemission peaks labeled A–F. Panel (b) shows the local density of states, displaying the individual contributions from the Cu $3d$, $4s$, and O $2p$ electrons.

TABLE III. The ion clamped static macroscopic dielectric constant, ϵ_∞ , as calculated with selected DFT methods used as the reference Hamiltonian within the G_0W_0 method. Values in parentheses were calculated treating Cu semicore electrons explicitly.

Functional	Ion clamped static macroscopic dielectric constant, ϵ_∞
PBE	8.58 (7.99)
PBE+ U	6.15 (5.90)
PBE0	3.70 (3.76)
HSE	4.84 (4.85)
Experiment	6.46 ^a

^aReference 51.

Discrepancies between the calculated quasiparticle peaks and experimental removal energies in Table II may arise from our use of a unit cell representing the bulk material in the GW calculations, which does not take into account the effects of surface states on the PES/IPES. Additionally, our values for the quasiparticle peaks are referenced to the valence band maximum, so any error in calculating the valence band maximum will shift all peaks erroneously. This effect can be seen most strongly in the quasiparticle peaks from PBE+ G_0W_0 , where the underestimation of the removal energies of all electrons is most likely due to an underestimation of the direct gap, leading to a more positive valence band maximum, shifting all peaks positively.

The HSE+ G_0W_0 total and projected DOS plots are shown in Fig. 2. These projected DOSs illustrate the character of the states which contribute to the electron removal energies observed via photoemission. It is clear that the O $2p$ electrons are the main contributor to the states in the lower-energy region ranging from -8 to -5 eV, whereas the higher-energy region ranging from -4 to 0 eV is mainly of Cu $3d$ character, with some hybridization with O $2p$ states and contributions from Cu $4s$ states at the edge of the valence band.

As an additional test of the choice of reference Hamiltonian within the G_0W_0 method, the ion clamped static macroscopic dielectric constant ϵ_∞ was computed within the RPA, and compared to the measured value in Table III. PBE+ U shows the greatest accuracy in calculating ϵ_∞ , while its value is underestimated by the hybrid functionals and overestimated by PBE. Because PBE overdelocalizes electrons in strongly correlated materials, the too high dielectric constant (too large screening) is to be expected. It is evident that the hybrid functionals produce consistent values independent of explicit inclusion

of the semicore electrons, whereas the value for ϵ_∞ is more strongly dependent on the number of electrons in the calculation when using PBE and PBE+ U . This parallels the trend observed in the dependence of the electron removal energies on the inclusion of the semicore electrons, further illustrating the stability of the hybrid functionals. The underestimation of ϵ_∞ by HSE may simply reflect shortcomings of the RPA in calculating screening, but the impact of the error is minimized by the improved accuracy of HSE in generating input wave functions and eigenvalues.

The HSE+ G_0W_0 approach is therefore an accurate means of predicting PE/IPE gaps and PE spectra for cuprous oxide. This also serves as the starting point for determination of the OAS, which can be accomplished through the use of methods such as the Bethe-Salpeter equations, which account for the electron-hole interactions in neutral excitations. Such calculations are beyond the scope of the present work and are left for further study.

IV. CONCLUSIONS

To conclude, we have shown that a perturbative G_0W_0 approach is appropriate for understanding the electronic properties of Cu₂O, as long as the correct reference Hamiltonian is chosen. Through a thorough survey of common DFT-based approaches and XC functionals, we have established the HSE functional as the most accurate in reproducing a number of experimental observables, confirming it as the proper functional for studying ground-state properties of Cu₂O. This is because Cu₂O is a mixed character insulator, necessitating a portion of exact exchange treatment of all electrons to produce the correct ground-state electronic structure. The combined HSE+ G_0W_0 approach has also been established here as a proper tool to reproduce and analyze PE/IPE data, as well as to serve as the starting point for studies of the OAS. Finally, we have shown that explicit treatment of semicore electrons is unnecessary when using higher levels of theory such as hybrid functionals in the reference Hamiltonian.

ACKNOWLEDGMENTS

E.A.C. acknowledges the support of the Air Force Office of Scientific Research for funding and the DoD High Performance Computing Modernization Program at the NAVY, AFRL, and ERDC DSRC for supercomputer time. L.Y.I. is grateful to the National Science Foundation for a graduate fellowship.

*Author to whom all correspondence should be addressed: eac@princeton.edu

¹S. Brahm, S. Nikitine, and J. P. Dahl, *Phys. Lett.* **22**, 31 (1966).

²F. Caballero-Briones, J. M. Artés, I. Díez-Pérez, P. Gorostiza, and F. Sanz, *J. Phys. Chem. C* **113**, 1028 (2009).

³K. Klier, in *Advances in Catalysis* (Elsevier, Amsterdam, 1982), pp. 243–313.

⁴R. Zhou, T. Yu, X. Jiang, F. Chen, and X. Zheng, *Appl. Surf. Sci.* **148**, 263 (1999).

⁵M. Hara, T. Kondo, M. Komoda, S. Ikeda, J. N. Kondo, K. Domen, M. Hara, K. Shinohara, and A. Tanaka, *Chem. Commun.* **357** (1998).

⁶P. E. de Jongh, D. Vanmaekelbergh, and J. J. Kelly, *Chem. Commun.* **1069** (1999).

- ⁷J. Frese, *J. Electrochem. Soc.* **138**, 3338 (1991).
- ⁸M. Le, M. Ren, Z. Zhang, P. T. Sprunger, R. L. Kurtz, and J. C. Flake, *J. Electrochem. Soc.* **158**, E45 (2011).
- ⁹M. C. Toroker, D. K. Kanan, N. Alidoust, L. Y. Isseroff, P. Liao, and E. A. Carter, *Phys. Chem. Chem. Phys.* **13**, 16644 (2011).
- ¹⁰V. T. Agekyan, *Phys. Status Solidi A* **43**, 11 (1977).
- ¹¹P. W. Baumeister, *Phys. Rev.* **121**, 359 (1961).
- ¹²L. Hedin, *Phys. Rev.* **139**, A796 (1965).
- ¹³S. V. Faleev, M. van Schilfgaarde, and T. Kotani, *Phys. Rev. Lett.* **93**, 126406 (2004).
- ¹⁴M. S. Hybertsen and S. G. Louie, *Phys. Rev. B* **34**, 5390 (1986).
- ¹⁵E. L. Shirley, *Phys. Rev. B* **54**, 7758 (1996).
- ¹⁶M. van Schilfgaarde, T. Kotani, and S. Faleev, *Phys. Rev. Lett.* **96**, 226402 (2006).
- ¹⁷T. Kotani, M. van Schilfgaarde, and S. V. Faleev, *Phys. Rev. B* **76**, 165106 (2007).
- ¹⁸P. Romaniello, S. Guyot, and L. Reining, *J. Chem. Phys.* **131**, 154111 (2009).
- ¹⁹M. Shishkin, M. Marsman, and G. Kresse, *Phys. Rev. Lett.* **99**, 246403 (2007).
- ²⁰F. Bruneval, N. Vast, L. Reining, M. Izquierdo, F. Sirotti, and N. Barrett, *Phys. Rev. Lett.* **97**, 267601 (2006).
- ²¹S. Hüfner, *Adv. Phys.* **43**, 183 (1994).
- ²²P. Liao and E. A. Carter, *Phys. Chem. Chem. Phys.* **13**, 15189 (2011).
- ²³V. I. Anisimov, J. Zaanen, and O. K. Andersen, *Phys. Rev. B* **44**, 943 (1991).
- ²⁴S. L. Dudarev, A. I. Liechtenstein, M. R. Castell, G. A. D. Briggs, and A. P. Sutton, *Phys. Rev. B* **56**, 4900 (1997).
- ²⁵H. Jiang, R. Gomez-Abal, P. Rinke, and M. Scheffler, *Phys. Rev. B* **82**, 045108 (2010).
- ²⁶E. Kioupakis, P. Zhang, M. L. Cohen, and S. G. Louie, *Phys. Rev. B* **77**, 155114 (2008).
- ²⁷C. Adamo and V. Barone, *J. Chem. Phys.* **110**, 6158 (1999).
- ²⁸J. Heyd, G. E. Scuseria, and M. Ernzerhof, *J. Chem. Phys.* **118**, 8207 (2003).
- ²⁹J. Heyd and G. E. Scuseria, *J. Chem. Phys.* **120**, 7274 (2004).
- ³⁰J. Heyd and G. E. Scuseria, *J. Chem. Phys.* **121**, 1187 (2004).
- ³¹J. Heyd, J. E. Peralta, G. E. Scuseria, and R. L. Martin, *J. Chem. Phys.* **123**, 174101 (2005).
- ³²J. P. Perdew, K. Burke, and M. Ernzerhof, *Phys. Rev. Lett.* **77**, 3865 (1996).
- ³³J. P. Perdew, K. Burke, and M. Ernzerhof, *Phys. Rev. Lett.* **78**, 1396 (1997).
- ³⁴C. Rödl, F. Fuchs, J. Furthmüller, and F. Bechstedt, *Phys. Rev. B* **79**, 235114 (2009).
- ³⁵G. Kresse and D. Joubert, *Phys. Rev. B* **59**, 1758 (1999).
- ³⁶F. D. Murnaghan, *Proc. Natl. Acad. Sci. USA* **30**, 244 (1944).
- ³⁷P. E. Blöchl, O. Jepsen, and O. K. Andersen, *Phys. Rev. B* **49**, 16223 (1994).
- ³⁸D. M. Ceperley and B. J. Alder, *Phys. Rev. Lett.* **45**, 566 (1980).
- ³⁹J. P. Perdew and A. Zunger, *Phys. Rev. B* **23**, 5048 (1981).
- ⁴⁰S. L. Dudarev, G. A. Botton, S. Y. Savrasov, C. J. Humphreys, and A. P. Sutton, *Phys. Rev. B* **57**, 1505 (1998).
- ⁴¹A. V. Krukau, O. A. Vydrov, A. F. Izmaylov, and G. E. Scuseria, *J. Chem. Phys.* **125**, 224106 (2006).
- ⁴²Z.-X. Shen, R. S. List, D. S. Dessau, F. Parmigiani, A. J. Arko, R. Bartlett, B. O. Wells, I. Lindau, and W. E. Spicer, *Phys. Rev. B* **42**, 8081 (1990).
- ⁴³J. Ghijsen, L. H. Tjeng, J. van Elp, H. Eskes, J. Westerink, G. A. Sawatzky, and M. T. Czyzyk, *Phys. Rev. B* **38**, 11322 (1988).
- ⁴⁴A. Martinez-Ruiz, M. G. Moreno, and N. Takeuchi, *Solid State Sci.* **5**, 291 (2003).
- ⁴⁵M. Nolan and S. D. Elliott, *Phys. Chem. Chem. Phys.* **8**, 5350 (2006).
- ⁴⁶J. Paier, M. Marsman, K. Hummer, G. Kresse, I. C. Gerber, and J. G. Angyan, *J. Chem. Phys.* **124**, 154709 (2006).
- ⁴⁷J. M. Zuo, M. Kim, M. O’Keeffe, and J. C. H. Spence, *Nature (London)* **401**, 49 (1999).
- ⁴⁸A. Filippetti and V. Fiorentini, *Phys. Rev. B* **72**, 035128 (2005).
- ⁴⁹A. Werner and H. D. Hochheimer, *Phys. Rev. B* **25**, 5929 (1982).
- ⁵⁰M. M. Beg and S. M. Shapiro, *Phys. Rev. B* **13**, 1728 (1976).
- ⁵¹M. O’Keeffe, *J. Chem. Phys.* **39**, 1789 (1963).